Where is the Hidden Intramolecular H-bonding Vibrational Signal in the Proline Matrix IR Spectrum?

James Langford, Yuzhe Zhang, Zehua Chen, and Yang Yang*

Theoretical Chemistry Institute and Department of Chemistry, University of Wisconsin-Madison, Madison, Wisconsin 53706, United States.

Email: yyang222@wisc.edu

Abstract

The assignment of the hydrogen bonded O-H stretch vibration in the proline matrix IR spectrum has sparked controversy. Employing constrained nuclear electronic orbital methods, we provide a clear assignment that the vibrational frequency drops to near 3000 cm^{-1} as a result of the interplay between electronic effects, nuclear quantum effects, and matrix effects.

Hydrogen bonding interactions play a crucial role in a variety of biological systems, impacting critical biological processes such as protein folding and enzyme catalysis.[1–5] Recently, nuclear quantum effects (NQEs) have been shown to be an important factor that modulates the properties of hydrogen bonds, especially within enzyme active sites.[6–10] Given that amino acids and short peptides are the fundamental building blocks of proteins, it is essential to develop a comprehensive understanding of the hydrogen bonding interactions in these systems and of the influence of NQEs on these hydrogen bonds. However, the impact of NQEs on the

hydrogen bonding of amino acids and short peptides remains largely unexplored, representing an important direction for research.

Among the proteinogenic amino acids, proline asserts a singular influence over protein structure and function due to its unique ring structure.[11,12] Unlike other amino acids, proline's side chain is covalently bonded to the nitrogen, thereby forming a characteristic pyrrolidine loop.[11,13] Consequently, proline can disrupt and terminate both alpha helices and beta sheets[11,12,14–17] as well as form a distinct type of protein secondary structure known as a polyproline helix.[12,18,19] Furthermore, beyond its biological functions, proline can act as a catalyst in important organic reactions such as the aldol and Mannich reactions.[20–22]

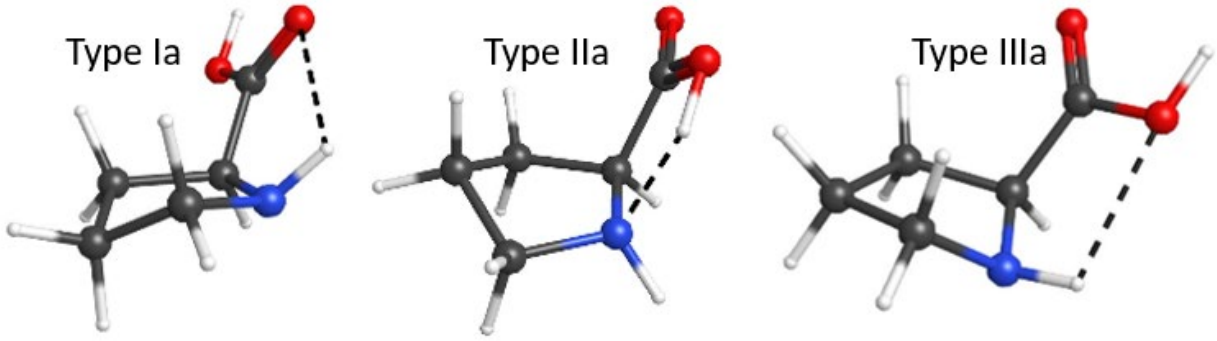

Figure 1. Three major types of proline conformers with different hydrogen bonding interactions, which are depicted by dashed lines.

As with other amino acids, proline can exist in multiple conformers, which can be categorized by their intramolecular hydrogen bonding patterns as shown in Figure 1.[13,23–30] Type I features an N−H···O=C interaction, Type II features an H−N···H−O interaction, and Type III features an N−H···O-H interaction.[13,23–30] Types I and III are characterized by hydrogen bonded N-H stretches and free O-H stretches, while Type II is characterized by a free N-H stretch and a hydrogen bonded O-H stretch. Typically, Type I and Type III conformers are highly similar in their vibrational spectra, and we here collectively refer to them as Type I/III. The

ring structure of proline introduces an additional source of conformational isomerism. Specifically, the pyrrolidine ring can pucker either up or down, with the lower-case letters *a* and *b* used to refer to the lower and higher energy ring puckers, respectively.[13] The energy ordering of these conformers can vary depending on the amino acid. For proline, past experimental and theoretical investigations indicate that the Type II conformer is the lowest in energy, and that the lower-energy ring-pucker conformers dominate under the experimental matrix conditions.[13,31–40]

Amino acid conformers can be investigated with vibrational spectroscopy. Experimentally, gas-phase FT-IR results are available, but these experiments are conducted at high temperatures, which tend to break hydrogen bonds and thus eliminate the distinction between conformers.[41] In contrast, matrix isolation spectroscopy is conducted at cryogenic temperatures within a frozen inert gas matrix.[42–44] These experimental conditions stabilize different types of conformers, allowing them to be identified through the obtained IR spectra.[42–44] It has been observed that, in general, the O-H stretching frequencies for Type I, Type II, and Type III amino acids are highly consistent when measured within the same matrix conditions.[13] For instance, in argon matrices at approximately 12 K, the free O-H stretches for Type I and Type III amino acids appear near 3560 cm^{-1}, and the hydrogen-bonded O-H stretch for Type II appears near 3200 cm^{-1}.[13,25–30,45–59]

However, experimental studies on proline did not yield any identifiable signal near 3200 cm^{-1},[13,60] even though computationally, Type IIa proline is shown to be the lowest-energy conformer, and experimentally, two peaks occur in the C=O

stretch region, which are believed to correspond to the Type Ia/IIIa and Type IIa conformers.[13,60] This raises a perplexing question: where is the proline Type IIa hydrogen-bonded O-H vibrational signal in the matrix IR spectrum?

Adamowicz and co-workers originally proposed that this signal appears in the C-H stretching region and is thus obscured by the C-H stretch peaks.[13] This assignment was based on the experimental difference spectrum between proline (proline-D_0) and doubly deuterated proline (proline-D_2, with N-H and O-H deuterated), which shows a broad peak centered at 3025 cm^{-1}.[13] Computationally, density functional theory (DFT)-based harmonic analysis with an empirical scale factor of 0.92 yielded a frequency of 3031 cm^{-1}, which further supported this assignment.[13] However, pure DFT-based harmonic analysis is unable to capture anharmonicity and NQEs, and is of questionable reliability when using empirical scale factors to account for these effects.

Recently, using the adiabatically switched semiclassical initial value representation (AS-SCIVR),[39,61–63] a new assignment was proposed, suggesting that the Type IIa hydrogen bonded O-H stretch is at 3329 cm^{-1},[39] near the previously assigned N-H stretching region and significantly outside the C-H stretching region.[13,60] However, this new peak assignment is also not fully convincing, as the experimental spectra show only a weak and broad N-H stretch signal in the 3300-3400 cm^{-1} region,[13,60] and it would be unusual if this weak signal could correspond to both O-H and N-H stretches.

In this work, we will identify this missing and disputed Type IIa hydrogen bonded O-H stretch signal in the matrix IR spectrum of proline through constrained

nuclear-electronic orbital (CNEO)[64–66] calculations. The CNEO framework, which was recently developed in our group, can incorporate NQEs, especially quantum nuclear delocalization effects, in quantum chemistry calculations and molecular dynamics simulations through a quantum-corrected effective potential energy surface.[67,68] This framework has been shown to be remarkably successful for hydrogen-related vibrations.[69–73] Herein, our study will provide strong evidence supporting the original assignment of the Type IIa hydrogen bonded O-H stretch as appearing within the C-H stretching region as a result of the interplay between electronic effects, NQEs, and matrix effects.

Table 1. O-H Stretching Frequencies (cm^{-1}) in Type IIa Proline

Experiment[a]	CNEO[b]		VPT2[b]	AS-SCIVR[c]	Conventional DFT[b]		
	DFT	MD			Unscaled	Scaled[d]	AIMD
3025 (disputed)	3021	3036	3069	3329	3359	3090	3382

a. Experimental value from difference spectrum in reference 13

b. Values obtained in this work with B3LYP/aug-cc-pVDZ

c. AS-SCIVR value from reference 39, obtained with B3LYP-D3/aug-cc-pVDZ

d. Value from this work with scale factor of 0.92 from reference 13 applied.

The hydrogen bonded O-H vibrational frequencies for the Type IIa proline conformer are provided in Table 1. The disputed experimental result is 3025 cm^{-1}, which is the maximum position of a wide and relatively faint peak in the difference spectrum of proline-D_0 and proline-D_2. Without NQEs, unscaled DFT/B3LYP harmonic analysis predicts the frequency to be 3359 cm^{-1}, which is about 300 cm^{-}

^{1} higher than the experimental assignment. When the empirical scale factor of 0.92 as used by Adamowicz and co-workers is applied,[13] the frequency drops sharply to 3090 cm^{-1}. However, the reliability of empirical scale factors can be questionable, as they often need to vary with vibrational modes as well as electronic structure methods. With AS-SCIVR, this hydrogen bonded O-H vibrational frequency was reported to be 3329 cm^{-1},[39] which is similar to the unscaled DFT harmonic result and does not support the experimental assignments.

Using the same B3LYP functional[74–76] as selected in previous works,[13,34,39,62] we performed both VPT2[77,78] calculations and CNEO-DFT harmonic analysis. The predicted frequencies of the Type IIa hydrogen-bonded O-H stretch are 3069 cm^{-1} and 3021 cm^{-1} for VPT2 and CNEO-DFT, respectively. These predictions align with the original experimental difference spectrum assignment and scaled DFT harmonic analysis by Adamowicz and co-workers.[13] We note that our current study and the original study by Adamowicz did not include dispersion corrections whereas the AS-SCIVR study used D3 corrections. One might expect that dispersion corrections are needed as hydrogen bonds are not real chemical bonds. However, the necessity of dispersion corrections for hydrogen-bonded systems is less clear-cut compared to other weak interaction systems, since the nature of hydrogen bonding is more electrostatic than dispersion.[79] To further support this treatment, we provide the DFT harmonic results and VPT2 results with the D3(0)[80] and D3(BJ)[81] corrections, along with the corresponding DFT and VPT2 values without the corrections, in Table S3. This analysis shows that essentially the

dispersion correction can only change the frequencies by at most ~30 cm^{-1}, which can be neglected compared to the peak assignment dispute of around 200 cm^{-1}.

According to previous studies by our group on hydrogen-related vibrations, CNEO-DFT harmonic analysis can reduce errors by 90% compared to conventional unscaled DFT harmonic analysis.[66,69–71] Furthermore, although VPT2 may face challenges with strongly hydrogen-bonded systems or shared-proton systems,[70,82] the hydrogen bond in Type IIa proline is comparatively weaker, with its expected vibrational frequency being above 3000 cm^{-1}. Therefore, VPT2 is reliable for this system. The agreement between the CNEO-DFT harmonic frequencies and the corresponding VPT2 values indicates that this assignment is robust. However, to achieve even more accurate results, we additionally performed CNEO-MD simulations. Compared to CNEO harmonic analysis, CNEO-MD can better capture mode coupling effects through thermal motions at finite temperatures and therefore yield more accurate peak positions and qualitatively correct peak broadenings;[69–71] however, we acknowledge that the descriptions of overtones, combination bands, and Fermi resonances are still challenging and that high-level quantum methods, such as MCTDH and VSCF/VCI, are still needed for accurate descriptions of these subtle features.[70,71] The improved performance of CNEO-MD over CNEO-DFT harmonic analysis is usually more significant for hydrogen-bonded O-H stretch modes, which often couple strongly with some low-frequency vibrations, than it is for free O-H stretches, which have relatively weak couplings to other modes.[70,71]

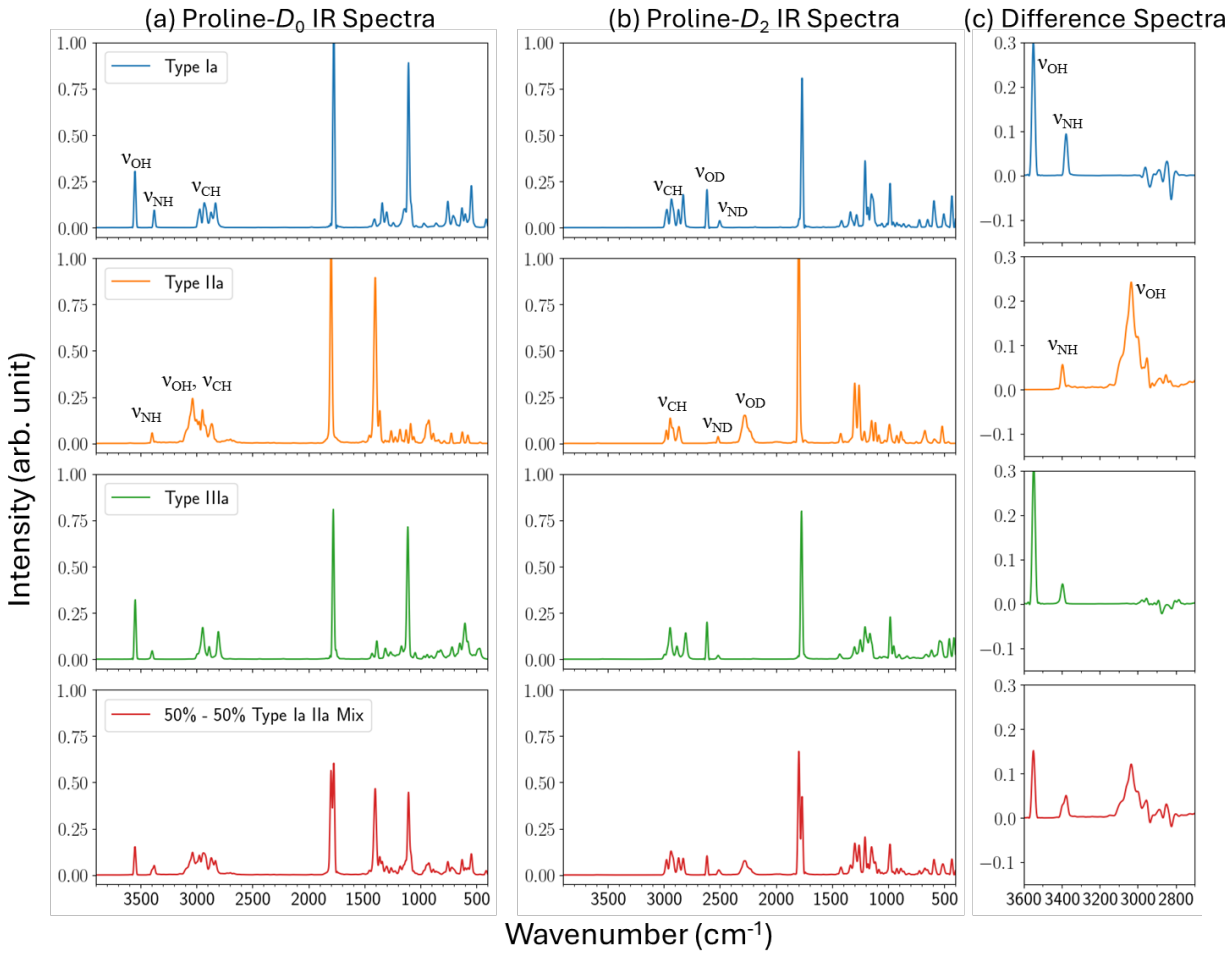

Figure 2. Simulated IR spectra by CNEO-MD-B3LYP for different types of conformers of (a) un-deuterated proline-D_0 and (b) doubly deuterated proline-D_2. Panel (c) shows the difference between (a) and (b) in the high frequency 2600–3600 cm^{-1} region.

The CNEO-MD simulated IR spectra for both un-deuterated proline-D_0 and doubly deuterated proline-D_2 are shown in Figures 2(a) and 2(b), respectively. For each species, we performed MD simulations for the lowest energy Type IIa conformer as well as the Type Ia and Type IIIa conformers. The Fourier transform is applied to the dipole autocorrelation functions of the MD trajectories to obtain their respective IR spectra. To compare with the experimental spectra, which are believed to be a mixture of mainly the Type Ia and Type IIa conformers, we also created mixed spectra for both proline-D_0 and proline-D_2 with a 50%-50% mixing ratio. In principle, if equilibrium is reached, the mixing ratio should follow a

Boltzmann distribution. However, since the experiment involved first sublimating the amino acid—potentially breaking hydrogen bonds and allowing bond rotation—and then cooling it down to a matrix environment, the relative ratio of different conformers formed and stabilized during the cooling process is uncertain.[83] For qualitative investigation, we simply chose a 50% Type Ia and 50% Type IIa mixing ratio. Our peak assignments for the Type Ia and Type IIa conformers are shown in the spectra.

For both the Type Ia and Type IIIa conformers, the un-deuterated proline-D_0 and doubly deuterated proline-D_2 CNEO-MD IR spectra show great resemblance above the fingerprint region, except for the strong O-H stretch and weak N-H stretch peaks, which shift to lower frequencies upon deuteration. In contrast, for the Type IIa conformer, while the weak N-H(D) stretch remains clear in both the un-deuterated and deuterated species, the O-H stretch does not display a distinct single peak in the un-deuterated species. Fortunately, the O-D stretch in proline-D_2 is distinct with a peak lower in frequency than the N-D stretch. This peak serves as evidence that in the un-deuterated species, the Type IIa hydrogen bonded O-H stretch frequency is also very likely lower than that for the N-H stretch and thus likely appears close to the C-H stretch region around 3000 cm^{-1}.

Upon further examination of the C-H stretch region in the CNEO-MD spectra, we can clearly observe differences between proline-D_0 and proline-D_2 for the Type IIa conformer. The progression of bands around 3000 cm^{-1} is distinctly broader and stronger in the proline-D_0 spectrum than that in the proline-D_2 spectrum. In contrast, for the Type Ia and Type IIIa conformers, the two species have essentially the

same line shape and intensities for both isotopes in the C-H stretch region. These observations suggest that the Type IIa hydrogen-bonded O-H stretch overlaps with the C-H stretch region.

This assignment is further supported by the simulated CNEO-MD difference spectra shown in Figure 2(c). For each conformer, the difference spectrum was obtained by subtracting that conformer's CNEO-MD calculated proline-D_0 spectrum from the corresponding proline-D_2 spectrum. Because the OH, NH, and CH stretch modes are of the main interest, we show the difference spectra focused in on the 2700 cm^{-1} to 3600 cm^{-1} range. For the Type IIa difference spectrum, a clear and broadened peak is observed with a maximum intensity at 3036 cm^{-1}, whereas the difference in this same region is essentially negligible for the Type Ia and Type IIIa conformers.

Quantitatively, the simulated difference spectra for both the Type IIa conformer and the 1:1 Type Ia-IIa conformer mixture show a narrower broadening compared to the experimental result, with a peak broadening of about 200 cm^{-1} in our simulations versus about 400 cm^{-1} in the experiment. Several factors could contribute to this difference. One is that the choice of the electronic functional can affect the peak position as well as the mode couplings. Another factor is that these simulations are performed in the pure gas phase, which neglects the matrix environment that might also couple with the molecular modes and further broaden the spectrum. Both factors will be discussed in more detail in the following paragraphs. Nonetheless, the qualitative similarity in peak broadening and the consistent peak centering near the experimental value of 3025 cm^{-1} strongly

support the conclusion that the Type IIa hydrogen-bonded O-H stretch overlaps with the C-H stretch region.

Furthermore, we performed conventional DFT-based AIMD simulations as a comparison. The results are presented in Figure S1. AIMD gives a peak value of 3382 cm^{-1} for the Type IIa hydrogen bonded O-H stretch, which is more than 300 cm^{-1} higher than the CNEO-MD result and is significantly separated from the C-H stretch region. This large difference between the CNEO-MD and AIMD results demonstrates again the crucial role of quantum nuclear delocalization during MD simulations of hydrogen bonding systems.

In addition to nuclear quantum effects and mode coupling effects, matrix effects in experiments and the electronic structure method used in computations influence the alignment between experimental spectra and theoretical predictions. In experiments, the molecule is frozen within an inert gas matrix, which typically weakens the bonds and causes a redshift in the corresponding vibrational frequencies.[84,85] This effect is particularly significant for hydrogen-bonded O-H stretches.[84] Previous studies of glycine, the simplest amino acid, have shown that different inert gas matrices can produce varying redshifts due to the varying coupling strength between the matrix gas and the amino acid.[47] Specifically, it was found that the argon (Ar) matrix can cause a redshift of nearly 100 cm^{-1} for the hydrogen bonded O-H stretch in the Type II glycine conformer.[47] Given the stronger basicity of the secondary amine in proline compared to the primary amine in glycine, we may anticipate a similar, if not greater, redshift for proline. Therefore, if a low temperature gas phase spectrum of proline were to be obtained via advanced

spectroscopic techniques like isotopomer-selective photofragmentation vibrational spectroscopy,[86,87] we expect that the hydrogen-bonded O-H stretch frequency would be around 100 cm^{-1} higher than the current matrix spectrum due to the absence of matrix effects. This would result in a clearer peak separation of the hydrogen bonded O-H stretch from the C-H stretch region.

For the electronic structure method, although the B3LYP functional is used in this study as well as in previous works, it is in fact not the most accurate electronic functional. To assess the error introduced by the electronic structure method, we performed harmonic analysis using coupled cluster singles and doubles (CCSD),[88] with the results shown in Table S1. Although harmonic analysis with CCSD does not account for NQEs, it can serve as a relatively accurate reference to assess errors in the electronic functional. Compared to the CCSD harmonic results, pure DFT-B3LYP harmonic analysis underestimates the hydrogen-bonded O-H stretch in Type IIa by 156 cm^{-1}, indicating that the B3LYP functional significantly underestimates the vibrational frequency. Therefore, although CNEO-CCSD is not yet developed, we anticipate that its predicted hydrogen bonded O-H vibration for Type IIa proline would be around 150 cm^{-1} higher than the result predicted by CNEO-B3LYP, resulting in a separation from the C-H stretch region. In addition to B3LYP, we performed harmonic analysis and MD simulations with the PBE0[89–91] and M06-2X[92] functionals (Table S2, Figures S2-S5). For PBE0, the overall performance is highly similar to B3LYP, with underestimated vibrational frequencies relative to CCSD. A major difference is that CNEO-MD with PBE0 gives an even broader peak than that with B3LYP, which

aligns better with the matrix experimental result. In contrast, M06-2X suffers less from functional error and predicts vibrational frequencies similar to CCSD. As a result, CNEO-MD simulated spectra with M06-2X see a distinct peak separation between the hydrogen-bonded O-H stretch and the C-H stretches.

Interestingly, the 100 cm^{-1} or more redshift caused by experimental matrix effects and the 150 cm^{-1} functional underestimation relative to CCSD due to the choice of the B3LYP functional play nearly the same role of shifting the hydrogen bonded O-H stretch into the C-H stretch region, leading to a fortuitous match between the matrix IR experiment spectrum and the simulated CNEO-B3LYP-MD spectrum. If pure gas phase IR spectra of proline are recorded, without matrix effects, we estimate the hydrogen bonded O-H stretch will better separate from the C-H stretch region as predicted by CNEO-MD using the more accurate M06-2X functional.

Given that the proline Type IIa hydrogen bonded O-H stretch has been unequivocally assigned, now the remaining question is: why is this frequency significantly redshifted to around 3000 cm^{-1} compared to the 3200 cm^{-1} results observed for other amino acids? A reasonable explanation was provided by Adamowicz et al. in their original paper: because secondary amines are more nucleophilic than primary amines, the corresponding N···H−O hydrogen bond in proline will be stronger than those in other amino acids. This stronger hydrogen bond weakens the O-H bond more and thus leads to a lower O-H vibrational frequency.

We further support this explanation by comparing the optimized geometries of Type IIa proline and with Type II glycine. With CNEO-DFT, the O-H and N···H distances are 1.031 Å and 1.711 Å for proline, and 0.986 Å and 1.924 Å for glycine. The longer O-H distance and shorter N···H distance in proline indicate a stronger hydrogen bond compared to glycine. Similar results are also observed with conventional DFT-optimized geometries (0.991 Å proline O-H, 1.868 Å proline N···H, 0.986 Å glycine O-H, 1.924 Å glycine N···H), leading to consistent conclusions.

In summary, by employing CNEO methods to account for NQEs in proline, we have unequivocally assigned the Type IIa proline hydrogen-bonded O-H stretch to a broad peak overlapping with the C-H stretch region near 3000 cm^{-1}. CNEO-DFT harmonic analysis qualitatively supports this assignment, and the CNEO-MD difference spectrum result further confirms the broad O-H stretching peak observed experimentally with the predicted central peak position in good alignment with the experimental difference spectrum. We find that experimental matrix effects and electronic errors in the employment of the B3LYP functional in computations both lead to a redshift of 100 cm^{-1} or more for the Type IIa hydrogen bonded O-H stretch peak position, contributing to the overlap with the C-H stretch region and thereby aligning computational predictions with experimental results. The unique secondary amine group in proline, with its high nucleophilicity, accounts for the stronger hydrogen bond and weakened O-H bond in its Type IIa conformer, which is the primary reason for the significantly redshifted peak position compared to other amino acids.

Supplementary Material

Computational details and example input files, functional benchmark tests, complete O-H stretch vibrational frequencies and vibrational spectra by different methods, and effects of dispersion corrections.

Acknowledgment

Funding support from the National Science Foundation under Grant No. 2238473 and from the University of Wisconsin via the Wisconsin Alumni Research Foundation. Calculations were performed using the resources provided by high performance cluster of the Center for High Throughput Computing at the University of Wisconsin – Madison.[93]

Data Availability

The data that supports the findings of this study are available within the article and its Supplementary Materials. More detailed data are available from the corresponding author upon reasonable request.

References

(1) Narlikar, G. J.; Herschlag, D. Mechanistic Aspects Of Enzymatic Catalysis: Lessons from Comparison of RNA and Protein Enzymes. *Annu. Rev. Biochem.* **1997**, *66* (1), 19–59. https://doi.org/10.1146/annurev.biochem.66.1.19.

(2) Bruice, T. C.; Benkovic, S. J. Chemical Basis for Enzyme Catalysis. *Biochemistry* **2000**, *39* (21), 6267–6274. https://doi.org/10.1021/bi0003689.

(3) Benkovic, S. J.; Hammes-Schiffer, S. A Perspective on Enzyme Catalysis. *Science* **2003**, *301* (5637), 1196–1202. https://doi.org/10.1126/science.1085515.

(4) Hubbard, R. E.; Kamran Haider, M. Hydrogen Bonds in Proteins: Role and Strength. In *eLS*; John Wiley & Sons, Ltd, 2010. https://doi.org/10.1002/9780470015902.a0003011.pub2.

(5) Herschlag, D.; Pinney, M. M. Hydrogen Bonds: Simple after All? *Biochemistry* **2018**, *57* (24), 3338–3352. https://doi.org/10.1021/acs.biochem.8b00217.
(6) Hwang, J.-K.; Warshel, A. How Important Are Quantum Mechanical Nuclear Motions in Enzyme Catalysis? *J. Am. Chem. Soc.* **1996**, *118* (47), 11745–11751. https://doi.org/10.1021/ja962007f.
(7) Pu, J.; Gao, J.; Truhlar, D. G. Multidimensional Tunneling, Recrossing, and the Transmission Coefficient for Enzymatic Reactions. *Chem. Rev.* **2006**, *106* (8), 3140–3169. https://doi.org/10.1021/cr050308e.
(8) Wang, L.; Fried, S. D.; Boxer, S. G.; Markland, T. E. Quantum Delocalization of Protons in the Hydrogen-Bond Network of an Enzyme Active Site. *Proceedings of the National Academy of Sciences* **2014**, *111* (52), 18454–18459. https://doi.org/10.1073/pnas.1417923111.
(9) Vardi-Kilshtain, A.; Nitoker, N.; Major, D. T. Nuclear Quantum Effects and Kinetic Isotope Effects in Enzyme Reactions. *Archives of Biochemistry and Biophysics* **2015**, *582*, 18–27. https://doi.org/10.1016/j.abb.2015.03.001.
(10) Markland, T. E.; Ceriotti, M. Nuclear Quantum Effects Enter the Mainstream. *Nat Rev Chem* **2018**, *2* (3), 1–14. https://doi.org/10.1038/s41570-017-0109.
(11) Madison, V. Flexibility of the Pyrrolidine Ring in Proline Peptides. *Biopolymers* **1977**, *16* (12), 2671–2692. https://doi.org/10.1002/bip.1977.360161208.
(12) Morgan, A. A.; Rubenstein, E. Proline: The Distribution, Frequency, Positioning, and Common Functional Roles of Proline and Polyproline Sequences in the Human Proteome. *PLOS ONE* **2013**, *8* (1), e53785. https://doi.org/10.1371/journal.pone.0053785.
(13) Stepanian, S. G.; Reva, I. D.; Radchenko, E. D.; Adamowicz, L. Conformers of Nonionized Proline. Matrix-Isolation Infrared and Post-Hartree−Fock Ab Initio Study. *J. Phys. Chem. A* **2001**, *105* (47), 10664–10672. https://doi.org/10.1021/jp011708i.
(14) Piela, L.; Némethy, G.; Scheraga, H. A. Proline-Induced Constraints in α-Helices. *Biopolymers* **1987**, *26* (9), 1587–1600. https://doi.org/10.1002/bip.360260910.
(15) Sankararamakrishnan, R.; Vishveshwara, S. Conformational Studies on Peptides with Proline in the Right-Handed α-Helical Region. *Biopolymers* **1990**, *30* (3–4), 287–298. https://doi.org/10.1002/bip.360300307.
(16) Li, S. C.; Goto, N. K.; Williams, K. A.; Deber, C. M. Alpha-Helical, but Not Beta-Sheet, Propensity of Proline Is Determined by Peptide Environment. *Proceedings of the National Academy of Sciences* **1996**, *93* (13), 6676–6681. https://doi.org/10.1073/pnas.93.13.6676.
(17) Deber, C. M.; Therien, A. G. Putting the β-Breaks on Membrane Protein Misfolding. *Nat Struct Mol Biol* **2002**, *9* (5), 318–319. https://doi.org/10.1038/nsb0502-318.
(18) Adzhubei, A. A.; Sternberg, M. J. E. Left-Handed Polyproline II Helices Commonly Occur in Globular Proteins. *Journal of Molecular Biology* **1993**, *229* (2), 472–493. https://doi.org/10.1006/jmbi.1993.1047.
(19) Adzhubei, A. A.; Sternberg, M. J. E.; Makarov, A. A. Polyproline-II Helix in Proteins: Structure and Function. *Journal of Molecular Biology* **2013**, *425* (12), 2100–2132. https://doi.org/10.1016/j.jmb.2013.03.018.
(20) Bahmanyar, S.; Houk, K. N. Origins of Opposite Absolute Stereoselectivities in Proline-Catalyzed Direct Mannich and Aldol Reactions. *Org. Lett.* **2003**, *5* (8), 1249–1251. https://doi.org/10.1021/ol034198e.
(21) Panday, S. K. Advances in the Chemistry of Proline and Its Derivatives: An Excellent Amino Acid with Versatile Applications in Asymmetric Synthesis. *Tetrahedron: Asymmetry* **2011**, *22* (20), 1817–1847. https://doi.org/10.1016/j.tetasy.2011.09.013.

(22) Sunoj, R. B. Proline-Derived Organocatalysis and Synergism between Theory and Experiments. *WIREs Computational Molecular Science* **2011**, *1* (6), 920–931. https://doi.org/10.1002/wcms.37.
(23) Suenram, R. D.; Lovas, F. J. Millimeter Wave Spectrum of Glycine. A New Conformer. *J. Am. Chem. Soc.* **1980**, *102* (24), 7180–7184. https://doi.org/10.1021/ja00544a002.
(24) Hu, C. H.; Shen, M.; Schaefer, H. F. I. Glycine Conformational Analysis. *J. Am. Chem. Soc.* **1993**, *115* (7), 2923–2929. https://doi.org/10.1021/ja00060a046.
(25) Ivanov, A. Y.; Sheina, G.; Blagoi, Yu. P. FTIR Spectroscopic Study of the UV-Induced Rotamerization of Glycine in the Low Temperature Matrices (Kr, Ar, Ne). *Spectrochimica Acta Part A: Molecular and Biomolecular Spectroscopy* **1998**, *55* (1), 219–228. https://doi.org/10.1016/S1386-1425(98)00288-1.
(26) Stepanian, S. G.; Reva, I. D.; Radchenko, E. D.; Rosado, M. T. S.; Duarte, M. L. T. S.; Fausto, R.; Adamowicz, L. Matrix-Isolation Infrared and Theoretical Studies of the Glycine Conformers. *J. Phys. Chem. A* **1998**, *102* (6), 1041–1054. https://doi.org/10.1021/jp973397a.
(27) Stepanian, S. G.; Reva, I. D.; Radchenko, E. D.; Adamowicz, L. Conformational Behavior of α-Alanine. Matrix-Isolation Infrared and Theoretical DFT and Ab Initio Study. *J. Phys. Chem. A* **1998**, *102* (24), 4623–4629. https://doi.org/10.1021/jp973479z.
(28) Stepanian, S. G.; Reva, I. D.; Radchenko, E. D.; Adamowicz, L. Combined Matrix-Isolation Infrared and Theoretical DFT and Ab Initio Study of the Nonionized Valine Conformers. *J. Phys. Chem. A* **1999**, *103* (22), 4404–4412. https://doi.org/10.1021/jp984457v.
(29) Bazsó, G.; Najbauer, E. E.; Magyarfalvi, G.; Tarczay, G. Near-Infrared Laser Induced Conformational Change of Alanine in Low-Temperature Matrixes and the Tunneling Lifetime of Its Conformer VI. *J. Phys. Chem. A* **2013**, *117* (9), 1952–1962. https://doi.org/10.1021/jp400196b.
(30) Stepanian, S. G.; Ivanov, A. Yu.; Adamowicz, L. Conformational Composition of Neutral Leucine. Matrix Isolation Infrared and Ab Initio Study. *Chemical Physics* **2013**, *423*, 20–29. https://doi.org/10.1016/j.chemphys.2013.06.018.
(31) Ramek, M.; Kelterer, A.-M.; Nikolić, S. Ab Initio and Molecular Mechanics Conformational Analysis of Neutral L-Proline. *International Journal of Quantum Chemistry* **1997**, *65* (6), 1033–1045. https://doi.org/10.1002/(SICI)1097-461X(1997)65:6<1033::AID-QUA2>3.0.CO;2-W.
(32) Császár, A. G.; Perczel, A. Ab Initio Characterization of Building Units in Peptides and Proteins. *Progress in Biophysics and Molecular Biology* **1999**, *71* (2), 243–309. https://doi.org/10.1016/S0079-6107(98)00031-5.
(33) Lesarri, A.; Mata, S.; Cocinero, E. J.; Blanco, S.; López, J. C.; Alonso, J. L. The Structure of Neutral Proline. *Angewandte Chemie International Edition* **2002**, *41* (24), 4673–4676. https://doi.org/10.1002/anie.200290012.
(34) Czinki, E.; Császár, A. G. Conformers of Gaseous Proline. *Chemistry – A European Journal* **2003**, *9* (4), 1008–1019. https://doi.org/10.1002/chem.200390103.
(35) Allen, W. D.; Czinki, E.; Császár, A. G. Molecular Structure of Proline. *Chemistry – A European Journal* **2004**, *10* (18), 4512–4517. https://doi.org/10.1002/chem.200400112.
(36) Mata, S.; Vaquero, V.; Cabezas, C.; Peña, I.; Pérez, C.; C. López, J.; L. Alonso, J. Observation of Two New Conformers of Neutral Proline. *Physical Chemistry Chemical Physics* **2009**, *11* (21), 4141–4144. https://doi.org/10.1039/B904633J.
(37) Fathi, F.; Farrokhpour, H. Valence Ionization of L-Proline Amino Acid: Experimental and Theoretical Study. *Chemical Physics Letters* **2013**, *565*, 102–107. https://doi.org/10.1016/j.cplett.2013.02.032.
(38) Hadidi, R.; Božanić; Ganjitabar, H.; Garcia, G. A.; Powis, I.; Nahon, L. Conformer-Dependent Vacuum Ultraviolet Photodynamics and Chiral Asymmetries in Pure Enantiomers of Gas

Phase Proline. *Commun Chem* **2021**, *4* (1), 1–14. https://doi.org/10.1038/s42004-021-00508-z.
(39) Botti, G.; Aieta, C.; Conte, R. The Complex Vibrational Spectrum of Proline Explained through the Adiabatically Switched Semiclassical Initial Value Representation. *J. Chem. Phys.* **2022**, *156* (16), 164303. https://doi.org/10.1063/5.0089720.
(40) Yang, Y.; Lin, Z. Extensive Exploration of the Conformational Landscapes of Neutral and Terminally Blocked Prolines in the Gas Phase: A Density Functional Theory Study. *Journal of Chemical Research* **2022**, *46* (4), 17475198221110480. https://doi.org/10.1177/17475198221110480.
(41) Linder, R.; Nispel, M.; Häber, T.; Kleinermanns, K. Gas-Phase FT-IR-Spectra of Natural Amino Acids. *Chemical Physics Letters* **2005**, *409* (4), 260–264. https://doi.org/10.1016/j.cplett.2005.04.109.
(42) Bally, T. Matrix Isolation. In *Reactive Intermediate Chemistry*; Moss, R. A., Platz, M. S., Jones Jr., M., Eds.; John Wiley & Sons, Ltd, 2003; pp 795–845. https://doi.org/10.1002/0471721492.ch17.
(43) Dubey, P.; Saini, J.; Verma, K.; Karir, G.; Mukhopadhyay, A.; Viswanathan, K. S. Chapter 14 - Matrix Isolation Spectroscopy—A Window to Molecular Processes. In *Molecular and Laser Spectroscopy*; Gupta, V. P., Ed.; Elsevier, 2018; pp 317–340. https://doi.org/10.1016/B978-0-12-849883-5.00014-0.
(44) Dinu, D. F.; Podewitz, M.; Grothe, H.; Loerting, T.; Liedl, K. R. On the Synergy of Matrix-Isolation Infrared Spectroscopy and Vibrational Configuration Interaction Computations. *Theor Chem Acc* **2020**, *139* (12), 174. https://doi.org/10.1007/s00214-020-02682-0.
(45) Grenie, Y.; Lassegues, J.; Garrigou-Lagrange, C. Infrared Spectrum of Matrix-Isolated Glycine. *The Journal of Chemical Physics* **1970**, *53* (7), 2980–2982. https://doi.org/10.1063/1.1674426.
(46) Grenie, Y.; Garrigou-Lagrange, C. Infrared Spectra of Glycine Isotopic Species Isolated in an Argon or Nitrogen Matrix. *Journal of Molecular Spectroscopy* **1972**, *41* (2), 240–248. https://doi.org/10.1016/0022-2852(72)90204-4.
(47) Huisken, F.; Werhahn, O.; Ivanov, A. Yu.; Krasnokutski, S. A. The O–H Stretching Vibrations of Glycine Trapped in Rare Gas Matrices and Helium Clusters. *The Journal of Chemical Physics* **1999**, *111* (7), 2978–2984. https://doi.org/10.1063/1.479580.
(48) Lambie, B.; Ramaekers, R.; Maes, G. On the Contribution of Intramolecular H-Bonding Entropy to the Conformational Stability of Alanine Conformations. *Spectrochimica Acta Part A: Molecular and Biomolecular Spectroscopy* **2003**, *59* (6), 1387–1397. https://doi.org/10.1016/S1386-1425(02)00353-0.
(49) Lambie, B.; Ramaekers, R.; Maes, G. Conformational Behavior of Serine: An Experimental Matrix-Isolation FT-IR and Theoretical DFT(B3LYP)/6-31++G** Study. *J. Phys. Chem. A* **2004**, *108* (47), 10426–10433. https://doi.org/10.1021/jp047192v.
(50) Ramaekers, R.; Pajak, J.; Lambie, B.; Maes, G. Neutral and Zwitterionic Glycine.H2O Complexes: A Theoretical and Matrix-Isolation Fourier Transform Infrared Study. *The Journal of Chemical Physics* **2004**, *120* (9), 4182–4193. https://doi.org/10.1063/1.1643735.
(51) Ramaekers, R.; Pajak, J.; Rospenk, M.; Maes, G. Matrix-Isolation FT-IR Spectroscopic Study and Theoretical DFT(B3LYP)/6–31++G** Calculations of the Vibrational and Conformational Properties of Tyrosine. *Spectrochimica Acta Part A: Molecular and Biomolecular Spectroscopy* **2005**, *61* (7), 1347–1356. https://doi.org/10.1016/j.saa.2004.10.003.
(52) Jarmelo, S.; Lapinski, L.; Nowak, M. J.; Carey, P. R.; Fausto, R. Preferred Conformers and Photochemical (λ > 200 Nm) Reactivity of Serine and 3,3-Dideutero-Serine In the Neutral Form. *J. Phys. Chem. A* **2005**, *109* (25), 5689–5707. https://doi.org/10.1021/jp0511202.

(53) Kaczor, A.; Reva, I. D.; Proniewicz, L. M.; Fausto, R. Importance of Entropy in the Conformational Equilibrium of Phenylalanine: A Matrix-Isolation Infrared Spectroscopy and Density Functional Theory Study. *J. Phys. Chem. A* **2006**, *110* (7), 2360–2370. https://doi.org/10.1021/jp0550715.
(54) Dobrowolski, J. Cz.; Jamróz, M. H.; Kołos, R.; Rode, J. E.; Sadlej, J. Theoretical Prediction and the First IR Matrix Observation of Several L-Cysteine Molecule Conformers. *ChemPhysChem* **2007**, *8* (7), 1085–1094. https://doi.org/10.1002/cphc.200600784.
(55) Espinoza, C.; Szczepanski, J.; Vala, M.; Polfer, N. C. Glycine and Its Hydrated Complexes: A Matrix Isolation Infrared Study. *J. Phys. Chem. A* **2010**, *114* (18), 5919–5927. https://doi.org/10.1021/jp1014115.
(56) Bazsó, G.; Magyarfalvi, G.; Tarczay, G. Tunneling Lifetime of the Ttc/VIp Conformer of Glycine in Low-Temperature Matrices. *J. Phys. Chem. A* **2012**, *116* (43), 10539–10547. https://doi.org/10.1021/jp3076436.
(57) Boeckx, B.; Nelissen, W.; Maes, G. Potential Energy Surface and Matrix Isolation FT-IR Study of Isoleucine. *J. Phys. Chem. A* **2012**, *116* (12), 3247–3258. https://doi.org/10.1021/jp212240p.
(58) Boeckx, B.; Maes, G. The Conformational Behavior and H-Bond Structure of Asparagine: A Theoretical and Experimental Matrix-Isolation FT-IR Study. *Biophysical Chemistry* **2012**, *165–166*, 62–73. https://doi.org/10.1016/j.bpc.2012.03.006.
(59) Najbauer, E. E.; Bazsó, G.; Apóstolo, R.; Fausto, R.; Biczysko, M.; Barone, V.; Tarczay, G. Identification of Serine Conformers by Matrix-Isolation IR Spectroscopy Aided by Near-Infrared Laser-Induced Conformational Change, 2D Correlation Analysis, and Quantum Mechanical Anharmonic Computations. *J. Phys. Chem. B* **2015**, *119* (33), 10496–10510. https://doi.org/10.1021/acs.jpcb.5b05768.
(60) Reva, I. D.; Stepanian, S. G.; Plokhotnichenko, A. M.; Radchenko, E. D.; Sheina, G. G.; Blagoi, Yu. P. Infrared Matrix Isolation Studies of Amino Acids. Molecular Structure of Proline. *Journal of Molecular Structure* **1994**, *318*, 1–13. https://doi.org/10.1016/0022-2860(93)07907-E.
(61) Conte, R.; Parma, L.; Aieta, C.; Rognoni, A.; Ceotto, M. Improved Semiclassical Dynamics through Adiabatic Switching Trajectory Sampling. *J. Chem. Phys.* **2019**, *151* (21), 214107. https://doi.org/10.1063/1.5133144.
(62) Botti, G.; Ceotto, M.; Conte, R. On-the-Fly Adiabatically Switched Semiclassical Initial Value Representation Molecular Dynamics for Vibrational Spectroscopy of Biomolecules. *J. Chem. Phys.* **2021**, *155* (23), 234102. https://doi.org/10.1063/5.0075220.
(63) Conte, R.; Ceotto, M. Semiclassical Molecular Dynamics for Spectroscopic Calculations. In *Quantum Chemistry and Dynamics of Excited States*; John Wiley & Sons, Ltd, 2020; pp 595–628. https://doi.org/10.1002/9781119417774.ch19.
(64) Xu, X.; Yang, Y. Full-Quantum Descriptions of Molecular Systems from Constrained Nuclear–Electronic Orbital Density Functional Theory. *J. Chem. Phys.* **2020**, *153* (7), 074106. https://doi.org/10.1063/5.0014001.
(65) Xu, X.; Yang, Y. Constrained Nuclear-Electronic Orbital Density Functional Theory: Energy Surfaces with Nuclear Quantum Effects. *The Journal of Chemical Physics* **2020**, *152* (8), 084107. https://doi.org/10.1063/1.5143371.
(66) Xu, X.; Yang, Y. Molecular Vibrational Frequencies from Analytic Hessian of Constrained Nuclear–Electronic Orbital Density Functional Theory. *J. Chem. Phys.* **2021**, *154* (24), 244110. https://doi.org/10.1063/5.0055506.
(67) Chen, Z.; Yang, Y. Incorporating Nuclear Quantum Effects in Molecular Dynamics with a Constrained Minimized Energy Surface. *J. Phys. Chem. Lett.* **2023**, *14* (1), 279–286. https://doi.org/10.1021/acs.jpclett.2c02905.

(68) Wang, Y.; Chen, Z.; Yang, Y. Calculating Vibrational Excited State Absorptions with Excited State Constrained Minimized Energy Surfaces. *J. Phys. Chem. A* **2023**, *127* (25), 5491–5501. https://doi.org/10.1021/acs.jpca.3c01420.
(69) Xu, X.; Chen, Z.; Yang, Y. Molecular Dynamics with Constrained Nuclear Electronic Orbital Density Functional Theory: Accurate Vibrational Spectra from Efficient Incorporation of Nuclear Quantum Effects. *J. Am. Chem. Soc.* **2022**, *144* (9), 4039–4046. https://doi.org/10.1021/jacs.1c12932.
(70) Zhang, Y.; Xu, X.; Yang, N.; Chen, Z.; Yang, Y. Describing Proton Transfer Modes in Shared Proton Systems with Constrained Nuclear–Electronic Orbital Methods. *The Journal of Chemical Physics* **2023**, *158* (23), 231101. https://doi.org/10.1063/5.0151544.
(71) Zhang, Y.; Wang, Y.; Xu, X.; Chen, Z.; Yang, Y. Vibrational Spectra of Highly Anharmonic Water Clusters: Molecular Dynamics and Harmonic Analysis Revisited with Constrained Nuclear-Electronic Orbital Methods. *J. Chem. Theory Comput.* **2023**, *19* (24), 9358–9368. https://doi.org/10.1021/acs.jctc.3c01037.
(72) Zhao, X.; Chen, Z.; Yang, Y. Constrained Nuclear-Electronic Orbital QM/MM Approach for Simulating Complex Systems with Quantum Nuclear Delocalization Effects Incorporated. ChemRxiv May 8, 2024. https://doi.org/10.26434/chemrxiv-2024-gk1ws.
(73) Xu, X. Constrained Nuclear-Electronic Orbital Density Functional Theory with a Dielectric Continuum Solvent Model. *J. Phys. Chem. A* **2023**, *127* (30), 6329–6334. https://doi.org/10.1021/acs.jpca.3c02507.
(74) Becke, A. D. Density-Functional Exchange-Energy Approximation with Correct Asymptotic Behavior. *Phys. Rev. A* **1988**, *38* (6), 3098–3100. https://doi.org/10.1103/PhysRevA.38.3098.
(75) Becke, A. D. Density-functional Thermochemistry. III. The Role of Exact Exchange. *J. Chem. Phys.* **1993**, *98* (7), 5648–5652. https://doi.org/10.1063/1.464913.
(76) Lee, C.; Yang, W.; Parr, R. G. Development of the Colle-Salvetti Correlation-Energy Formula into a Functional of the Electron Density. *Phys. Rev. B* **1988**, *37* (2), 785–789. https://doi.org/10.1103/PhysRevB.37.785.
(77) Barone, V. Anharmonic Vibrational Properties by a Fully Automated Second-Order Perturbative Approach. *J. Chem. Phys.* **2005**, *122* (1), 014108. https://doi.org/10.1063/1.1824881.
(78) Franke, P. R.; Stanton, J. F.; Douberly, G. E. How to VPT2: Accurate and Intuitive Simulations of CH Stretching Infrared Spectra Using VPT2+K with Large Effective Hamiltonian Resonance Treatments. *J. Phys. Chem. A* **2021**, *125* (6), 1301–1324. https://doi.org/10.1021/acs.jpca.0c09526.
(79) Boese, A. D. Density Functional Theory and Hydrogen Bonds: Are We There Yet? *ChemPhysChem* **2015**, *16* (5), 978–985. https://doi.org/10.1002/cphc.201402786.
(80) Grimme, S.; Antony, J.; Ehrlich, S.; Krieg, H. A Consistent and Accurate Ab Initio Parametrization of Density Functional Dispersion Correction (DFT-D) for the 94 Elements H-Pu. *J. Chem. Phys.* **2010**, *132* (15), 154104. https://doi.org/10.1063/1.3382344.
(81) Grimme, S.; Ehrlich, S.; Goerigk, L. Effect of the Damping Function in Dispersion Corrected Density Functional Theory. *Journal of Computational Chemistry* **2011**, *32* (7), 1456–1465. https://doi.org/10.1002/jcc.21759.
(82) Dzugan, L. C.; DiRisio, R. J.; Madison, L. R.; McCoy, A. B. Spectral Signatures of Proton Delocalization in H+(H2O)N=1−4 Ions. *Faraday Discuss.* **2018**, *212* (0), 443–466. https://doi.org/10.1039/C8FD00120K.
(83) Miller, T. F., III; Clary, D. C.; Meijer, A. J. H. M. Collision-Induced Conformational Changes in Glycine. *The Journal of Chemical Physics* **2005**, *122* (24), 244323. https://doi.org/10.1063/1.1927527.

(84) Huisken, F.; Kaloudis, M.; Vigasin, A. A. Vibrational Frequency Shifts Caused by Weak Intermolecular Interactions. *Chemical Physics Letters* **1997**, *269*, 235–243.
(85) Bludský, O.; Chocholoušová, J.; Vacek, J.; Huisken, F.; Hobza, P. Anharmonic Treatment of the Lowest-Energy Conformers of Glycine: A Theoretical Study. *The Journal of Chemical Physics* **2000**, *113* (11), 4629–4635. https://doi.org/10.1063/1.1288914.
(86) Heine, N.; Fagiani, M. R.; Rossi, M.; Wende, T.; Berden, G.; Blum, V.; Asmis, K. R. Isomer-Selective Detection of Hydrogen-Bond Vibrations in the Protonated Water Hexamer. *J. Am. Chem. Soc.* **2013**, *135* (22), 8266–8273. https://doi.org/10.1021/ja401359t.
(87) Yang, N.; Duong, C. H.; Kelleher, P. J.; Johnson, M. A.; McCoy, A. B. Isolation of Site-Specific Anharmonicities of Individual Water Molecules in the I−·(H2O)2 Complex Using Tag-Free, Isotopomer Selective IR-IR Double Resonance. *Chemical Physics Letters* **2017**, *690*, 159–171. https://doi.org/10.1016/j.cplett.2017.09.042.
(88) Shavitt, I.; Bartlett, R. J. *Many-Body Methods in Chemistry and Physics: MBPT and Coupled-Cluster Theory*; Cambridge University Press, 2009.
(89) Perdew, J. P.; Burke, K.; Ernzerhof, M. Generalized Gradient Approximation Made Simple. *Phys. Rev. Lett.* **1996**, *77* (18), 3865–3868. https://doi.org/10.1103/PhysRevLett.77.3865.
(90) Perdew, J. P.; Ernzerhof, M.; Burke, K. Rationale for Mixing Exact Exchange with Density Functional Approximations. *J. Chem. Phys.* **1996**, *105* (22), 9982–9985. https://doi.org/10.1063/1.472933.
(91) Adamo, C.; Barone, V. Toward Reliable Density Functional Methods without Adjustable Parameters: The PBE0 Model. *The Journal of Chemical Physics* **1999**, *110* (13), 6158–6170. https://doi.org/10.1063/1.478522.
(92) Zhao, Y.; Truhlar, D. G. The M06 Suite of Density Functionals for Main Group Thermochemistry, Thermochemical Kinetics, Noncovalent Interactions, Excited States, and Transition Elements: Two New Functionals and Systematic Testing of Four M06-Class Functionals and 12 Other Functionals. *Theor Chem Account* **2008**, *120* (1), 215–241. https://doi.org/10.1007/s00214-007-0310-x.
(93) Center for High Throughput Computing. Center for High Throughput Computing, 2006. https://doi.org/10.21231/GNT1-HW21.